arXiv:cond-mat/0407181v1 [cond-mat.supr-con] 7 Jul 2004

Determining the superconducting gap structure in Sr_2RuO_4 from sound attenuation studies below T_c

Pedro Contreras and Michael Walker
Department of Physics, University of Toronto, Toronto, ON M5S 1A7, Canada

Kirill Samokhin
Department of Physics, Brock University, St. Catharines, ON L2S 3A1, Canada

(Dated: February 2, 2008)

This work presents a quantitative theoretical study of the sound attenuation in the unconventional multiband superconductor Sr_2RuO_4 below the superconducting transition temperature T_c. Sound attenuation in this material is shown to have the remarkable property of being able to identify different nodal structures on different bands. The nodal structures on the γ band on the one hand, and on the α and β bands on the other, are both found to be characterized by the existence of point nodes, but are significantly different in their quantitative aspects.

PACS numbers:

I. INTRODUCTION

Sr_2RuO_4 is an unconventional superconductor which has a Fermi surface composed of three sheets, called the α, β, and γ sheets (i.e. it is an example of a multiband superconductor). There is considerable agreement as to the symmetry of the superconducting state, but there is as yet no consensus as to the nodal structure of the superconducting gap on the different sheets of the Fermi surface. The purpose of this article is first of all to develop a model of a possible nodal structure, and secondly to present a detailed quantitative analysis of an ultrasonic attenuation experiment[1] which confirms the essential features of the model. It is a remarkable feature of ultrasonic attenuation in Sr_2RuO_4 that it is able to distinguish different nodal structures on different sheets of the Fermi surface. It does this because different sound wave modes are sensitive to quasiparticles on different parts of the Fermi surface.

Sr_2RuO_4 has a layered square-lattice structure similar to that of many high-temperature copper-oxide superconductors[2]. The critical temperature varies strongly with impurity concentration, and can be as high as $T_c \approx 1.5$ K. Furthermore, the normal state displays Fermi liquid behavior. (see Refs. 3 and 4 for reviews of the properties of Sr_2RuO_4.) There is currently a reasonable consensus that in Sr_2RuO_4 the Cooper pairs form in a spin-triplet state which breaks time reversal symmetry[5,6,7], and that the broken time-reversal symmetry results from a two-component order parameter of E_u symmetry.

There is, however, no consensus concerning the detailed structure of the nodes in the superconducting gap. The current situation is reviewed in Ref. 4 where two promising scenarios are discussed. Both scenarios involve line nodes, which would give a low-temperature specific heat varying approximately linearly with temperature, in qualitative agreement with the observations of Ref. 8. In one scenario, horizontal line nodes in the superconducting gap are proposed[9,10,11] (note however that such horizontal line nodes are not stable and tend to become point nodes[12]). Qualitative arguments indicate that horizontal line nodes can be consistent with ultrasonic attenuation measurements.[1,13] Whether or not the angular dependence of the thermal conductivity measured in a magnetic field also provides evidence for horizontal line nodes is discussed in Ref. 4. Another potential scenario[14] is the presence of a very small gap along the [100] directions where the Fermi surface is close to the zone boundary. While such depressions of the gap in the [100] directions may exist, it is clear that these can not be responsible for the observed ultrasonic attenuation. General symmetry arguments (independent of model details) show that the interaction of transverse [100] phonons with quasiparticles having wavevectors in a [100] direction is zero.[13] Thus nodal structures not along the [100] direction must be present to explain ultrasonic attenuation measurement.

In Section II we give a detailed analysis of the nodal structure expected for a broken time-reversal symmetry state of triplet E_u symmetry; this analysis differs considerably from those given previously. Here, an important result is anticipated using a general argument. The starting point is the assumption of gap characterized by a d-vector of the form

$$\mathbf{d}^i(\mathbf{k}) = \mathbf{e_z}\Big(d_x^i(\mathbf{k}) + i\ d_y^i(\mathbf{k})\Big), \tag{1}$$

where the superscript i refers to the α, β, or γ part of the Fermi surface (see Fig. 1 below) and where d_x^i and d_y^i are real and are the two components of the order parameter on Fermi surface sheet i. The energies of the Bogoliubov quasiparticle excitations corresponding to this d-vector are

$$E^i(\mathbf{k}) = \sqrt{(\epsilon_{\mathbf{k}}^i)^2 + [\Delta^i(T)]^2\{[d_x^i(\mathbf{k})]^2 + [d_y^i(\mathbf{k})]^2\}}. \tag{2}$$

The nodal points, i.e. the points where the Bogoliubov quasiparticle energy is zero, determine the low-temperature thermodynamic properties.[15] These points

are determined by the equations

$$\epsilon^i_{\mathbf{k}} = 0, \quad d^i_x(\mathbf{k}) = 0, \quad d^i_y(\mathbf{k}) = 0. \tag{3}$$

For a given i, each of these three equations represents a surface in the three-dimensional $\mathbf{k}$ space. In general, two surfaces intersect, if they intersect at all, on a line. If a third surface intersects this line it will intersect it at a point. Thus, in general, the solution of the three Eqs. 3 for a given i will be a point. Hence, we should expect point nodes, if any, for a broken time-reversal symmetry state such as is being proposed for Sr_2RuO_4. Lines nodes might occur for very special values of the material parameters, but this would be a highly unusual occurrence and should not be expected.

As noted above, the main point of this article is to develop a detailed quantitative theory of the ultrasonic attenuation in Sr_2RuO_4 and to extract the details of the nodal structure of Sr_2RuO_4 from a comparison of the results of this calculation with the experimental ultrasonic attenuation results of Ref. 1. Some details of the electron-phonon interaction important for the calculation of ultrasonic attenuation are given at the end of Section II. It is of particular importance to recall that the measured[1] ultrasonic attenuation in Sr_2RuO_4 is exceptional in its extreme anisotropy. This extreme anisotropy has been shown in Ref. 13 to be due to the layered square-lattice structure of Sr_2RuO_4, and to occur only in the interaction of phonons with electrons in the γ band, but not with electrons in the α and β bands. It is this fact that allows the attenuation of the three modes, identified in Ref. 1 as the L[100], L[110], and T[110] modes, as being due to the interaction with γ-band quasiparticles. The approximate T^2 low-temperature variation of ultrasonic attenuation[1] of these three modes suggests that the attenuation is due to γ-band point nodes, a result that is confirmed in more detailed numerical calculations. (In general, line nodes and point nodes give an ultrasonic attenuation that varies as T and T^2 respectively in the low temperature limit – see Section III).

The electron-phonon interaction responsible for the attenuation of the L[100], L[110], and T[110] phonon modes turns out, however, to be exactly zero for the T[100] phonon mode, and the attenuation for this phonon mode has a different temperature dependence ($T^{1.4}$) from that of the other three modes. This suggests that the attenuation of the T[100] mode is due to interactions with quasiparticle in a different band (the α or β bands, or both). The model nodal structure that fits these is also a structure with point nodes, but with a very low gap on a horizontal line joining the point nodes. Thus the α- and/or β-band nodal structure would appear to be line-node-like at temperatures which are not too low, and would dominate the overall thermodynamic behavior. The model proposed here would therefore not be inconsistent with the approximately linear in T behavior of the specific heat observed in Ref. 8.

Section III gives details of the formulae used to calculate the ultrasonic attenuation as a function of temperature. Section IV compares the results of our numerical calculations with the experimental results and confirms the qualitative statements of the preceding paragraph. The two previous studies most closely related to ours are those of Refs. 16, and 17. Both are carried out using isotropic models, as are all the previous studies of ultrasound attenuation in superconductors that we are aware of. However as noted in Ref. 13 isotropic models can give a misleading idea of the position of the gap nodes in unconventional superconductors. Thus, the extension of the treatment of ultrasonic attenuation to the anisotropic case, as is done below, is essential for a correct identification of the nodal structure.

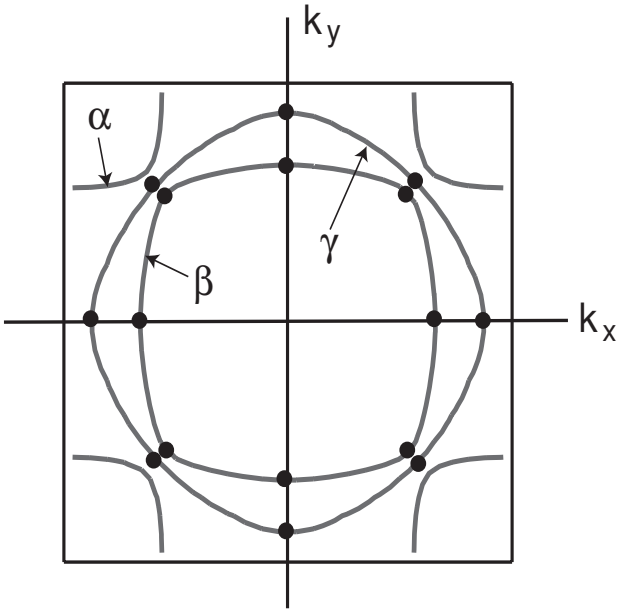

FIG. 1: The solid circles show the positions of the point nodes in the superconducting gap on the β and γ Fermi surface sheets in Sr_2RuO_4, as determined by Eqs. 7 and 8. Each solid circle represents two nodes, at positions $\pm k_z$. Evidence is presented in the article for the existence of point nodes in the γ band, and in the α or β bands, or both.

It has been shown some time ago[18] that the transport and thermal properties of heavy-fermion superconductors can be explained in terms of an effective electron scattering rate which except for the lowest temperatures, is approximately temperature independent and equal in magnitude to that of the normal state. Such a lifetime arises in a self-consistent treatment of impurity scattering near the unitary limit. Thus, in our treatment which is not self-consistent, we take the superconducting quasiparticle lifetime to be a constant and equal to that in the normal state (both being assumed to be due to impurity scattering). This approach has been found to be successful in ultrasonic attenuation studies in UPt_3, (see Ref. 19). A full self-consistent treatment solving for the anisotropic multiband gap function and energy-dependent scattering rate is beyond the scope of this article.

II. DETAILS OF THE SUPERCONDUCTING GAP AND THE ELECTRON-PHONON INTERACTION IN Sr_2RuO_4

The energy of a normal-state i-band electron ($i = \alpha, \beta, \gamma$) is periodic in reciprocal space, i. e. $\epsilon^i(\mathbf{k}) = \epsilon^i(\mathbf{k}+\mathbf{G})$ where $\mathbf{G}$ is any reciprocal lattice vector. This means that $\epsilon^i(\mathbf{k})$ can be written as a lattice Fourier series in the form

$$\epsilon^i(\mathbf{k}) \;=\; \sum_n \epsilon^i_n \; e^{i\,\mathbf{k}\cdot\mathbf{R_n}}, \tag{4}$$

where the sum is over all of the vectors $\mathbf{R_n}$ of the Bravais lattice. The particular form of this expression used in this article for the γ-band energy is the so called $t-t'$ approximation, (eg. see Ref. 23). In this approximation, electrons are assumed to hop between the Ru ions of a single layer of the Sr_2RuO_4 structure. Hopping between the layers is not allowed. The permitted intralayer hoppings are either nearest neighbor (matrix element t) or next-nearest neighbor (matrix element t'). This gives

$$\begin{aligned}\epsilon^\gamma_{\mathbf{k}} \;&=\; E_0 + 2t(\cos(k_x a) + \cos(k_y a)) + \\ &\quad 4t'\cos(k_x a)\cos(k_y a).\end{aligned} \tag{5}$$

The values for the γ-band tight binding parameters used in this paper are $(E_0 - E_F, t, t') = (-0.4, -0.4, -0.12)$

In a similar manner, the d-vector describing the superconducting gap in band i can be expanded as

$$\mathbf{d}^i(\mathbf{k}) \;=\; \sum_n \mathbf{d}^i_n \; e^{i\mathbf{k}\cdot\mathbf{R}_n}. \tag{6}$$

Here we adopt the view of Refs. 3,4 that the order parameter transforms as the E_u irreducible representation of the point group D_{4h} of Sr_2RuO_4, and that the state of E_u symmetry that is realized is one of broken time-reversal symmetry. The appropriate form of the d-vector is then given by Eq. 1. The explicit expressions that we use for d^i_x and d^i_y are

$$d^i_x(\mathbf{k}) = \delta^i \sin(k_x a) + \sin(\frac{k_x a}{2})\cos(\frac{k_y a}{2})\cos(\frac{k_z c}{2}), \tag{7}$$

and

$$d^i_y(\mathbf{k}) = \delta^i \sin(k_y a) + \cos(\frac{k_x a}{2})\sin(\frac{k_y a}{2})\cos(\frac{k_z c}{2}). \tag{8}$$

There are two different sets of basis vectors for the E_u representation occurring in Eqs. 7 and 8, one set contains the factor δ^i, and the second set contains the factor $\cos(k_z c/2)$. Related expressions for the d-vector have been given previously in Refs. 9,10,11, but always in combinations that give horizontal line nodes or no nodes. For example all the authors consider the case δ^i=0, which has horizontal line nodes at $k_z = \pm\,\pi/c$. However, any non-zero δ^i will remove the line nodes and produce instead point nodes. In order to fit the experimental results on ultrasound attenuation we will need quite a substantial value of δ^γ for the γ band and the point nodes in the γ band will play an important role. For the α and β bands the model of Eqs. 7 and 8 holds also, but it will be shown that δ^α or δ^β, or both, must be relatively small, but non-zero.

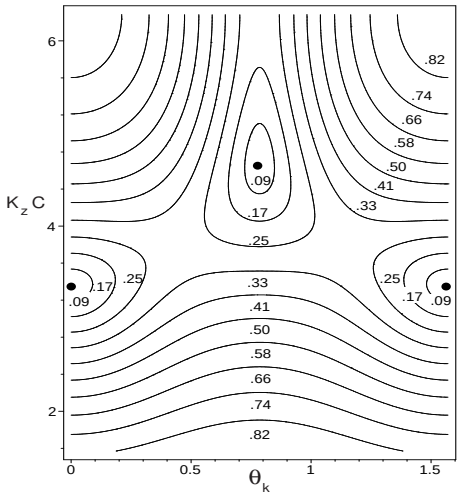

FIG. 2: Contour plot of the gap magnitude $|d^\gamma_{\mathbf{k}}|$ on the Fermi surface as a function of the longitudinal angle $\theta_{\mathbf{k}}$ relative to the [100] plane (see text), and $k_z c$ ($k_z c$ varies from $\pi/2$ to $2\,\pi$). The solid circles indicate the nodal points where the gap is zero.

To analyze in detail the nodal structure for Sr_2RuO_4, note that the Bogoliubov quasiparticle energy is given by Eq. 2. Clearly, for the superconducting energy gap to be zero on a given sheet i of the Fermi surface, the three Eqs. 3 must be satisfied. For non-zero δ^i in a certain range of values these equations have solutions, but only for $\mathbf{k}$ lying on the symmetry equivalent $\{100\}$ and $\{110\}$ planes. Assuming a solution exists, there are eight symmetry-related nodes in $\{100\}$ planes (see Fig. 1)for a given i; two of these nodal points are given by

$$k_z c = \pm 2\cos^{-1}[-2\delta^i\cos(k_x a/2)] \tag{9}$$

where $\mathbf{k} = (k_x, 0, k_z)$ lies on the Fermi surface. There are also eight symmetry-related nodes in $\{110\}$ planes for a given i; two of these nodal points are given by

$$k_z c = \pm 2\cos^{-1}(-2\delta^i) \tag{10}$$

where $\mathbf{k} = (k_x, k_x, k_z)$ lies on the Fermi surface as well (see Fig. 1 for details).

For these solutions to exist, we must have $|2\delta^i\cos(k_x a/2)| \le 1$ in the first case, and $|2\delta^i| \le 1$ in the second. Clearly, the existence of nodes in the second case implies their existence in the first case, but the nodes of the first case may or may not be accompanied by those of the second case. These point nodes are "accidental" in the sense that they are not required by symmetry, but exist only if the material parameters have values in a certain range. Also, these

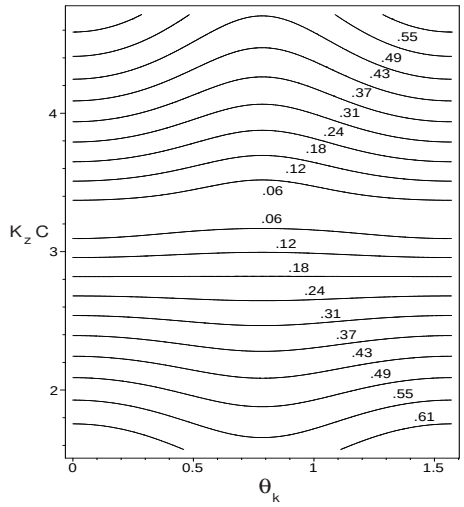

FIG. 3: Contour plot of the gap magnitude $|d^{\beta}_{\mathbf{k}}|$ on the Fermi surface as a function of the longitudinal angle $\theta_{\mathbf{k}}$ relative to the [100] plane (see text), and $k_z c$ ($k_z c$ varies from $\pi/2$ to $3/2\,\pi$).

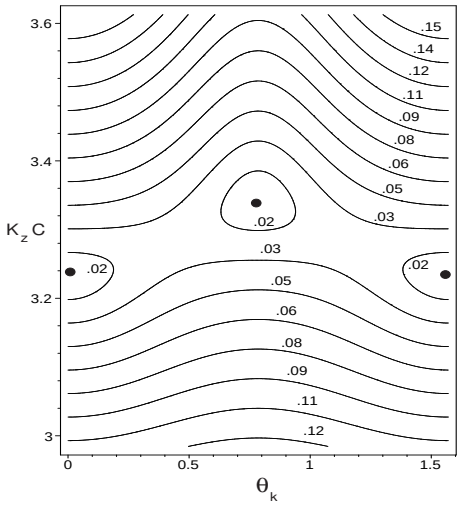

FIG. 4: Contour plot of the gap magnitude $|d^{\beta}_{\mathbf{k}}|$ on the Fermi surface as a function of the longitudinal angle $\theta_{\mathbf{k}}$ relative to the [100] plane (see text), and $k_z c$ ($k_z c$ varies from 0.95π to $1.15\,\pi$). The solid circles indicate the nodal points where the gap is zero.

point nodes will degenerate into the line nodes discussed by previous authors[9,10,11] if δ^i is exactly zero, but this should not in general be expected to be the case.

Contour plots of

$$|d^i_{\mathbf{k}}| = ([d^i_x(\mathbf{k})]^2 + [d^i_y\mathbf{k})]^2)^{1/2} \tag{11}$$

on the Fermi surface for both the γ and β bands are shown in Figs. 2, 3, and 4. This quantity is proportional to the magnitude of the gap at wave vector $\mathbf{k}$. To obtain a relatively simple graphical view of the nodal structure, the Fermi surfaces are parameterized using $\mathbf{k} = (\pi R\cos\theta_{\mathbf{k}}, \pi R\sin\theta_{\mathbf{k}}, k_z)$ with $R = 0.9$ for the γ band, and $R = 0.7$ for the β band [i.e. for this calculation the Fermi surfaces are approximated by right circular cylinders (c.f. Ref. 14)]. The values $\delta^\gamma = 0.35$ and $\delta^\beta = 0.05$, determined in Section IV by fitting the ultrasonic attenuation measurements to experiment, are used.

Notice (Fig. 2) that the γ band has well-defined point nodes with the gap rising to slightly less that one third of its maximum value between the nodes. When looked at on the same scale as the γ band, the β band appears to have line nodes (see Fig. 3). However, when looked on a finer scale (see Fig. 4), it is clear that the nodes in the β band are also point nodes, but that gap on a line between nodes is roughly ten times smaller than it is for the γ band. Thus, there are lines of very small gap for the β band.

Our calculation of the sound attenuation will make use of the electron-phonon matrix elements as determined in Ref. 13. As noted in the Introduction, the extremely anisotropic nature of the observed ultrasonic attenuation in Sr_2RuO_4 indicates[13] that the modes denoted as L[100], L[110], and T[110] in Ref. 1 are attenuated almost entirely by interactions with γ-band electrons. (L and T mean logitudinal and transverse, respectively, and the Miller indices give the direction of propagation.)

The appropriate electron-phonon matrix element for the L[100] mode is

$$f^{L[100]}(\mathbf{k}) = g^\gamma \cos(k_x a), \tag{12}$$

whereas for longitudinal [110] waves the matrix element is

$$f^{L[110]}(\mathbf{k}) = (g^\gamma/2)[\cos(k_x a) + \cos(k_y a)]. \tag{13}$$

For the transverse sound wave polarized in the basal plane and propagating in the [110] direction, the matrix element describing interactions with the γ-band electrons is

$$f^{T[110]}(\mathbf{k}) = (g^\gamma/2)[\cos(k_x a) - \cos(k_y a)] \tag{14}$$

Notice that the matrix elements for the longitudinal modes are nonzero at all of the point nodes in the γ band indicated in Fig. 1. Thus, all of the point nodes are "active" in the sense of Ref. 22, as is generally expected for longitudinal modes. Given that the low temperature ultrasonic attenuation is expected to vary roughly as T for line nodes and as T^2 for point nodes (see Section III), the experimentally observed temperature dependence[1] of $T^{1.8}$ for the longitudinal nodes indicates that the γ-band nodes are point nodes. Numerical studies confirm this conclusion (see Section IV). Similar conclusions are reached for the T[110] mode, but with the difference that its matrix element is non-zero for the [100] nodes, but zero for the [110] nodes. This confirms the existence of [100] point nodes in the γ band. According to the model discussed above, if [100] nodes exist, then [110] nodes exist also.

The attenuation of the T[100] mode, which is extremely weak, must be treated specially because, as described in Ref. 13, the dominant electron-phonon interaction for γ-band electrons (described above in terms of the interaction constant g^{γ}) is zero for T[100] phonons. Thus, the attenuation of this phonon mode must be due either to a different, weaker, interaction with γ-band electrons, e.g. described by the matrix element[13]

$$f^{T[100]}(\mathbf{k}) = g'^{\gamma} \sin(k_x a) \sin(k_y a), \tag{15}$$

or by an interaction with α- and/or β-band electrons. As described in Section IV, we have been unable to fit the temperature dependence of the T[100] attenuation by assuming an interaction of this mode with γ-band electrons. On the other hand, the attenuation of the T[100] mode can be accurately fit by assuming that it interacts predominantly with electrons in the α and β bands. For this to be the case it is necessary to choose the model parameters so that the gap on a line connecting α- and/or β-band point nodes is relatively small, so that at temperatures that are not too small the nodal structure of the α- and/or β-bands will appear somewhat line-like. This will provide consistency with a number of articles[4,8,9,10,11,14,20] where line nodes are assumed to exist to account for the thermodynamic properties of Sr_2RuO_4. The observed temperature dependence for the T[100] attenuation is $T^{1.4}$, which is in between the theoretical expectations for line and point nodes, as might be expected for line-like point nodes. An excellent quantitative fit the the experimental data for the T[100] mode, based on these ideas, is exhibited in Section IV.

III. CALCULATION OF THE SUPERCONDUCTING ULTRASOUND ATTENUATION

This article uses a standard formalism, extended to account for Fermi-surface and electron-phonon matrix-element anisotropy, to calculate the ultrasonic attenuation. This formalism is summarized here, and described in further detail in the Appendix of Ref. 13. A self-consistent calculation of the gap function and of the energy-dependent impurity scattering rate is beyond the scope of this article, which considers the incorporation of anisotropic effects into the more usual isotropic calculation as being the most essential for our purposes. Thus, in the superconducting state, we assume a constant energy-independent quasiparticle lifetime equal to that in the normal state. In early studies of heavy-fermion superconductivity, it was pointed out[18] that, so long as the temperature was not too low, such a quasiparticle scattering rate could account for the ultrasound and heat transport data in UPt_3. Similar results were found in Refs. 17,19. Therefore, the transport and thermal properties of heavy-fermion superconductors can be explained in terms of an effective electron scattering rate which except for the lowest temperatures, is approximately temperature independent and equal in magnitude to that of the normal state.

The expression that we use to calculate the ultrasonic attenuation is an expression valid at low frequencies where that ultrasonic attenuation is proportion to the square of the sound wave frequency, as is the case experimentally[1]. This expression, which is given in the appendix to Ref. 13, is

$$\frac{\alpha_j(\mathbf{q},T)}{\alpha_j(\mathbf{q},T_c)} = \int_0^{\infty} d\epsilon \left(-\frac{\partial f}{\partial \epsilon}\right) \frac{A_j^i(\mathbf{q},\epsilon)}{\epsilon}, \tag{16}$$

where

$$A_j^i(\mathbf{q},\epsilon) = \frac{\left\langle \tilde{f}_{j,\gamma}^2(\mathbf{k},\mathbf{q}) \,\mathrm{Re}\, \sqrt{\epsilon^2 - |\Delta_{\mathbf{k}}^{\gamma}|^2} \right\rangle_{FS}}{\left\langle \tilde{f}_{j,\gamma}^2(\mathbf{k},\mathbf{q}) \right\rangle_{FS}}. \tag{17}$$

and where j indicates the phonon mode, and $\langle\rangle_{FS}$ indicates a Fermi-surface average. It should be noted that, in order to preserve charge neutrality in the distorted lattice in the presence of a longitudinal sound wave[24], the electron-phonon matrix elements of the previous section must be replaced by effective matrix elements defined by

$$\tilde{f}^j(\mathbf{k}) = f^j(\mathbf{k}) - \left\langle f^j(\mathbf{k}) \right\rangle_{FS}. \tag{18}$$

in the formula for the ultrasonic attenuation.

Since we have not carried out a self-consistent evaluation of the gap, we do not have a model for the temperature dependence of the functions $\Delta^i(T)$ appearing in Eq. 2. In the absence of such a model, we simply assume a temperature dependence of the form $\Delta^i(T) = \Delta_0^i \sqrt{1-(T/T_c)^3}$, which is sometimes used in the literature (e.g. see Ref. 17). However, the choice of $\Delta(T)$ does not seem to affect our results, in particular we did not see any difference in the fits between $(T/T_c)^3$ and $(T/T_c)^2$.

It is useful for an initial interpretation of the ultrasonic attenuation data to have a simple expression for the expected temperature dependence of the attenuation at low temperatures for both line nodes and point nodes. For nodes that are "active" for a given phonon mode, the electron-phonon matrix element for that mode is by definition non-zero at the node and can be approximated by a constant, independent of wave vector, in the low-temperature limit. In this case, Eqs. 16 and 17 show that the ultrasonic attenuation in the low-temperature limit varies as

$$\alpha = C\, T \tag{19}$$

for line nodes, and

$$\alpha = C'\, T^2 \tag{20}$$

for point nodes, where C and C' are constants independent of temperature. For nodes that are inactive for a given phonon mode, these temperature dependences are one power of T higher.[22]

IV. QUANTITATIVE RESULTS

Fig. 5 shows the theoretical results for the temperature dependence of normalized ultrasonic attenuation calculated by evaluating Eq. 16, as well as the experimental results from Ref. 1, for the T[100],T[110], L[100], and L[110] modes. In obtaining the theoretical results, the parameters Δ_0^i and δ^i for $i = \gamma, \beta$ were determined in such a way as to give the best fit to the data.

First, the fitting of the data for the three relatively strongly attenuated phonon modes (L[100], L[110] and T[110]) [shown in panels (a), (b) and (c)] was attempted. The parameters $\Delta_0^\gamma = 0.7$ meV and $\delta^\gamma = 0.35$ gave excellent fits for the temperature dependence of all three modes. (The value of Δ^γ obtained here is in agreement with that maximum gap found in a recent scanning tunnelling microscopy experiment[21], showing at least that it has a reasonable order of magnitude.) The strong anisotropy in the attenuation (the mode viscosity of the L[110] mode is a factor of 30 smaller that that for the L[100] and T[110] modes) is not apparent in this figure since the attenuation relative to that at $T = T_c$ is plotted for each mode. It should be emphasized, however, that this anisotropy has been shown to be accurately accounted for by the assumed electron-phonon interaction, which (for these three modes) is characterized by a single constant, see Eqs. (12), (13), (14). This, as well as the excellent agreement between the theoretical and experimental temperature dependence for all three modes exhibited in Fig. 5, provides strong support for the essential features of the proposed model.

As a final step, we attempted to fit the temperature-dependent attenuation of the most weakly attenuated mode, the T[100] mode. As noted in Section II, the largest component of the electron-phonon interaction, which is responsible for the attenuation of the three modes discussed in the preceding paragraph, is exactly zero for the T[100] mode. Thus it is necessary to determine which new secondary electron-phonon interaction is appropriate for describing the attenuation of the T[100] mode, and in particular to which band the electrons contributing the most to this attenuation belong. (The theory of the different possible electron-phonon interactions is described in detail in Ref. 13). As a first attempt, the temperature-dependent attenuation was calculated using the electron-phonon matrix element of Eq. 15 and assuming that the dominant interaction is with electrons in the γ band. The result, shown in Fig. 5(d), gives a very poor fit to the experimental data. This should perhaps have been expected since the attenuation of the T[100] mode varies roughly as $T^{1.4}$ at low temperatures, in comparison with $T^{1.8}$ for the other three modes. Now, according to the theory, the limiting low-temperature temperature dependences should be determined by the nodal structure, so it is reasonable to assume that the attenuation of the T[100] modes is by its interaction with electrons in another band and with a different nodal structure, say the α or β band. Thus, we use the same model as used

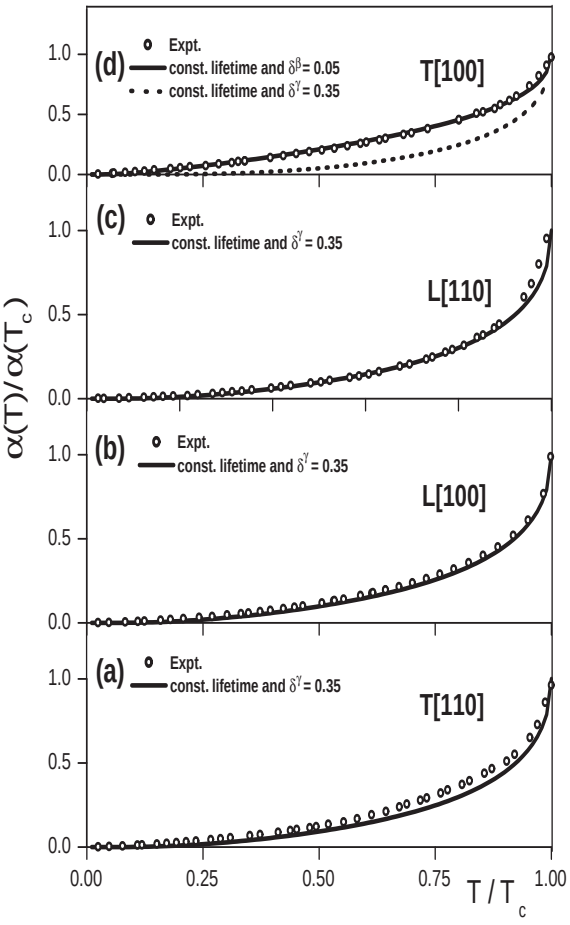

FIG. 5: Numerical fits of the in-plane ultrasound attenuation modes T[110], L[100], L[110], and T[100] normalized at T_c. Experimental data is taken from Ref.[1]. The free parameters are δ and Δ_0. The lifetime used to evaluate the expression for the attenuation is taken to be constant and equal to the one in the normal state.

for the other three modes, except that we allow the parameter δ^i (which here we call δ^β) in Eqs. 7 and 8 to vary so as to achieve the best fit with the data. The best value of this parameteris $\delta^\beta = 0.05$, and also $\Delta_0^\beta = 0.7$ meV. The nodal structure of the β band, calculated using this value of δ^β, is shown above in Figs. 3 and 4. Note that, although the nodes are point nodes, they have some of the properties of line nodes as there is a very low gap along the line joining the nodes. Hence, very roughly, this result suggests a temperature dependence for the attenuation somewhere between T (appropriate for line nodes) and T^2 (appropriate for point nodes) as is indeed the case.

V. CONCLUSIONS

A detailed quantitative interpretation of the temperature-dependent ultrasonic attenuation of Sr_2RuO_4 leads to the determination of essentially

different nodal structures on two different bands of this multi-band superconductor. This remarkable determination is possible because different phonon modes interact most strongly with electrons in different bands in this material. Furthermore, the exceptionally strong anisotropy in the attenuation of certain modes, which is unique to this material, allows one to associate the attenuation of the most strongly attenuated modes with their interaction with electrons in the γ band. Thus, the nodal structure of the γ band is found to be characterized by at least eight well-defined point nodes, symmetrically distributed in $\{100\}$ planes, and also by another eight point nodes, symmetrically distributed in $\{110\}$ planes. The attenuation of the most weakly attenuated mode gives information about the nodal structure of the α and β bands. The α/β band nodal structure is characterized by the existence of eight point nodes, symmetrically distributed in $\{110\}$ planes, in either or both of the α and β bands, and also by another eight point nodes symmetrically distributed in $\{100\}$ planes, in either or both of the α and β bands. The nodal structure here is, however, quantitatively different from that of the γ band, in that the gap on a line on the Fermi surface joining the nodes is an order of magnitude smaller than that on the γ band. This gives the α- and/or β-band nodal structures some of the characteristics of line nodes.

VI. ACKNOWLEDGMENTS

We thank L. Taillefer, M. Tanatar, I. Mazin, and W. Kim for stimulating discussions, and C. Lupien for providing us with the experimental data. We also thank the Canadian Institute for Advanced Research and the Natural Sciences and Engineering Research Council of Canada for their support. MBW thanks Efim Kats and the Theory Group of the Institute Laue Langevin (where part of this work was carried out) for their hospitality.

[1] C. Lupien, W. A. MacFarlane, C. Proust, L. Taillefer, Z. Q. Mao, and Y. Maeno, Phys. Rev. Lett. **86**, 5986 (2001).
[2] Y. Maeno, H. Hashimoto, K. Yoshida, S. Nishizaki, T. Fujita, J. G. Bednorz, and F. Lichtenberg, Nature **372**, 532 (1994).
[3] Y. Maeno, T. M. Rice, and M. Sigrist, Physics Today **54**, No. 1, 42 (2001).
[4] A. Mackenzie, and Y. Maeno, Rev. of Modern Physics **75**, 657 (2003).
[5] T. M. Rice and M. Sigrist, J. Phys. Condens. Matter **7**, L643 (1995).
[6] G. M. Luke, Y. Fudamoto, K. M. Kojima, M. I. Larkin, J. Merrin, B. Nachumi, Y. J. Uemura, Y. Maeno, Z. Q. Mao, H. Nakamura, and M. Sigrist, Nature **394**, 558 (1998).
[7] M. Walker and P. Contreras, Phys. Rev. B **66**, 214508 (2002).
[8] S. Nishizaki, Y. Maeno, and Z. Q. Mao, J. Low Temp. Phys. **117**, 1581 (1999).
[9] Y. Hasegawa, K. Machida, and M. Ozaki, J. Phys. Soc. Jpn. **69**, 336 (2000).
[10] M. Zhitomirsky and T. M. Rice, Phys. Rev. Lett. **87**, 057001-1 (2001).
[11] K. I. Wysokiński, G. Litak, J. F. Annett, and B. L. Györffy, Phys. Stat. Sol (b) **236**, 325 (2003).
[12] C. Bergemann, A. P. Mackenzie, S. R. Julian, D. Forsythe, and E. Omichi, Adv. Phys.**53**, 639 (2003).
[13] M. Walker, M. Smith, and K. Samokhin, Phys. Rev. B **65**, 014517-1 (2001).
[14] K. Miyake and O. Narikiyo, Phys. Rev. Lett. **83**, 1423 (1999).
[15] V. P. Mineev and K. V. Samokhin, *Introduction to Unconventional Superconductivity* (Gordon and Breach, Amsterdam, 1999).
[16] M. J. Graf and A. V. Balatsky, Phys. Rev. B **62**, 9697 (2000).
[17] W. C. Wu and R. Joynt, Phys. Rev. B **65**, 104502-1 (2002).
[18] S. Schmitt-Rink, K. Miyake, and C. M. Varma, Phys. Rev. Lett. **57** 2575 (1986).
[19] M. J. Graf, S.-K. Yip, and J. A. Sauls, Phys. Rev. B **62**, 14393 (2000).
[20] K. Deguchi, Z. Q. Mao, H. Yaguchi, and Y. Maeno, Phys. Rev. Lett. **92**, 047002-1-4 (2004).
[21] M. Upward, L. Kouwenhoven, A. Morpurgo, N. Kikugawa, Z. Mao, and Y. Maeno, Phys. Rev. B **65**, 220512-1 (2002).
[22] J. Moreno and P. Coleman, Phys. Rev. B **53**, R2995 (1996).
[23] I.I. Mazin and D. J. Singh, Phys. Rev. Lett. **79**, 733 (1997).
[24] A. I. Akhiezer, M. I. Kaganov, and G. Ia. Liubarskii, Sov. Phys. JETP **5**, 685 (1957).